

# 1 The global Deep-time Sediment Nitrogen Isotopes in 2 Marine Systems (DSMS-NI) database

3 Yong Du<sup>1</sup>, Huyue Song<sup>1,\*</sup>, Thomas J. Algeo<sup>1,2,3</sup>, Hui Zhang<sup>1</sup>, Jianwei Peng<sup>1</sup>, Yuyang  
4 Wu<sup>1,4</sup>, Jiankang Lai<sup>1</sup>, Xiang Shu<sup>1</sup>, Hanchen Song<sup>1</sup>, Lai Wei<sup>5</sup>, Jincheng Zhang<sup>6</sup>, Eva E.  
5 Stüeken<sup>7</sup>, Stephen E. Grasby<sup>8</sup>, Jacopo Dal Corso<sup>1</sup>, Xiaokang Liu<sup>1</sup>, Daoliang Chu<sup>1</sup>, Li  
6 Tian<sup>1</sup>, Qingzhong Liang<sup>6</sup>, Xinchuan Li<sup>6</sup>, Hong Yao<sup>6</sup>, Haijun Song<sup>1</sup>

7 <sup>1</sup>State Key Laboratory of Geomicrobiology and Environmental Changes, School of Earth Sciences,  
8 China University of Geosciences, Wuhan 430074, China

9 <sup>2</sup>Department of Geosciences, University of Cincinnati, Cincinnati, OH 45221-0013, USA

10 <sup>3</sup>State Key Laboratory of Oil and Gas Reservoir Geology and Exploitation, Chengdu University of  
11 Technology, Chengdu 610059, China

12 <sup>4</sup>College of Marine Science and Technology, China University of Geosciences, Wuhan 430074, China

13 <sup>5</sup>Shool of Future Technology, China University of Geosciences, Wuhan 430074, China

14 <sup>6</sup>School of Computer Science, China University of Geosciences, Wuhan 430074, China

15 <sup>7</sup>School of Earth & Environmental Sciences, University of St Andrews, St Andrews KY16 9AL, UK

16 <sup>8</sup>Geological Survey of Canada, Natural Resources Canada, Calgary, Alberta T2L 2A7, Canada

17 *Correspondence to:* Huyue Song (hysong@cug.edu.cn)

18 **Abstract.** Stable nitrogen isotope records preserved in marine sediments provide critical insights into  
19 Earth's climate history and biospheric evolution. Although numerous studies have documented nitrogen  
20 isotope ( $\delta^{15}\text{N}$ ) records for various geological systems (Archean to Recent) and paleogeographic settings,  
21 the scientific community remains constrained by the absence of a standardized database to  
22 systematically investigate their spatiotemporal evolution. Here, we present the database of Deep-time  
23 Sediment Nitrogen Isotopes in Marine Systems (DSMS-NI), a comprehensive global compilation of  
24  $\delta^{15}\text{N}$  data and associated geochemical parameters, spanning a vast collection of sediment samples  
25 dating from the Recent to the Archean. This database encompasses 70 854  $\delta^{15}\text{N}$  records derived from  
26 417 publications, systematically organized with 31 metadata fields categories (e.g., chronostratigraphic  
27 ages, coordinates, lithology, metamorphic grade, sedimentary facies, references) encompassing 1 999  
28 226 metadata. This repository further incorporates 130 proxy data fields, including 281 215  
29 geochemical data spanning total organic carbon (TOC), total nitrogen (TN), and organic carbon  
30 isotopes ( $\delta^{13}\text{C}_{\text{org}}$ ), major and trace elements and iron species. These integrated parameters enable

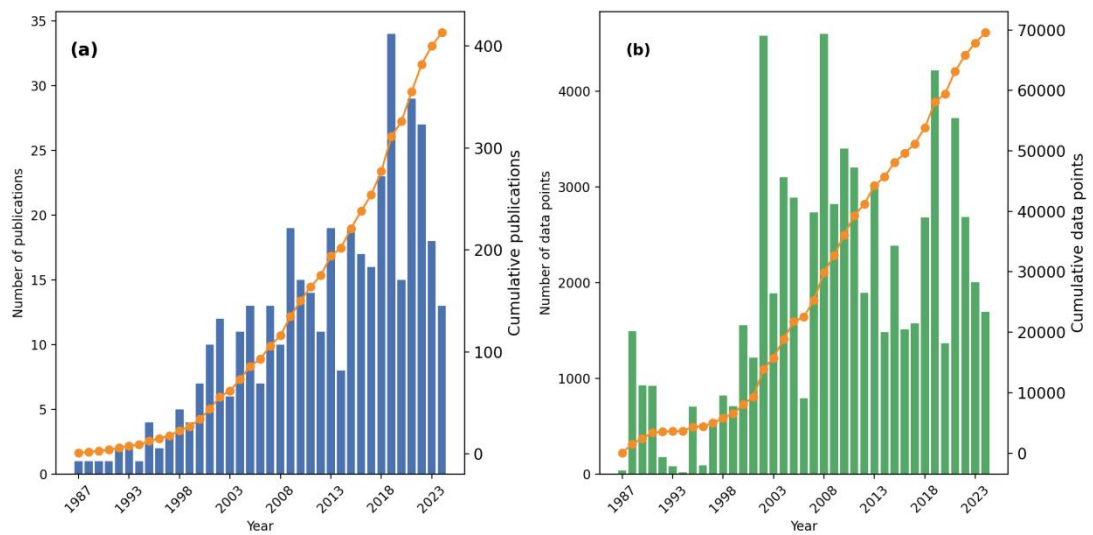
31 evaluation of sample fidelity and factors influencing  $\delta^{15}\text{N}$  signatures. The DSMS-NI database will  
32 facilitate research for key geological intervals such as the Permian/Triassic boundary and the  
33 Cretaceous oceanic anoxic events (OAEs). Researchers can leverage temporal and paleogeographic  
34 information, alongside geochemical data, to conduct spatiotemporal analyses, thereby uncovering  
35 changes in deep-time marine nitrogen cycles and paleoenvironmental conditions. The database is  
36 open-access via the Geobiology portal (<https://geobiologydata.cug.edu.cn/>, last access: 30 April 2025),  
37 allowing users to access data and submit new entries to ensure continuous updates and expansion. This  
38 resource represents a vital foundation for studies in paleoclimate, paleoenvironment, and geochemistry,  
39 offering essential data for understanding long-term Earth-system processes. The data files described in  
40 this paper are available at <https://doi.org/10.5281/zenodo.15117375> (Du et al., 2025a).

## 41 **1 Introduction**

42 Nitrogen, as an essential nutrient and redox-sensitive element, plays a crucial role in biological  
43 evolution and environmental climate changes (Ader et al., 2016; Pellerin et al., 2024). Typically,  
44 nitrogen isotope compositions are reported as a relative deviation of sample's isotopic ratio relative to  
45 that of atmospheric  $\text{N}_2$ , expressed in per mille (‰) as  $\delta^{15}\text{N} = (\text{R}_{\text{sample}}/\text{R}_{\text{AIR-N}_2} - 1) \times 1000$  ‰, where  $\text{R} =$   
46  $^{15}\text{N}/^{14}\text{N}$ . The  $\delta^{15}\text{N}$  record has become one of the primary tools for tracing the evolution of the nitrogen  
47 cycle and reconstructing redox conditions through deep time (Algeo et al., 2014; Sahoo et al., 2023; Du  
48 et al., 2024; Moretti et al., 2024). Advances in analytical techniques have facilitated rapid growth in the  
49 application of  $\delta^{15}\text{N}$  for paleoenvironmental studies in recent decades (Fig. 1; Zhong et al., 2023). Given  
50 nitrogen's short marine residence time of approximately 3000 years, which leads to regionally variable  
51 and rapidly shifting patterns (Gruber and Galloway, 2008), high-resolution  $\delta^{15}\text{N}$  datasets with detailed  
52 temporal and spatial coverage are critical for elucidating nitrogen cycle dynamics through Earth  
53 history.

54 Existing compilations of deep-time marine  $\delta^{15}\text{N}$  records exhibit significant limitations in term of  
55 temporal coverage and metadata compliance. Previous efforts have focused specifically on  
56 Precambrian to investigate the origins of microbial nitrogen metabolism and redox evolution during the  
57 Great Oxygenation Event (Thomazo et al., 2011; Stüeken et al., 2016, 2024; Kipp et al., 2018; Uveges  
58 et al., 2025). Other studies have targeted Phanerozoic systems (Algeo et al., 2014) or specific intervals  
59 such as the Paleozoic (Koehler et al., 2019), Cambrian (Wang et al., 2018; Liu et al., 2020),  
60 Carboniferous (Algeo et al., 2008), Triassic (Sun et al., 2024), and Cenozoic (Tesdal et al., 2013) to

61 analyze key biological and environmental events. The largest compilation of data from pre-Cenozoic  
 62 records contains fewer than 8 000  $\delta^{15}\text{N}$  entries (Stüeken et al., 2024). In contrast, Tesdal et al. (2013)  
 63 compiled up to 33 352 entries, but all of these records are from the past 6 million years. Moreover,  
 64 these repositories often fail to adhere systematically to the FAIR (Findable, Accessible, Interoperable,  
 65 Reusable) data principles (Wilkinson et al., 2016) and offer limited metadata categories. Typically, they  
 66 provide only broad geologic ages, lithology, and metamorphic grades, while lacking essential metadata  
 67 such as paleogeographic coordinates, depositional environments, and high-resolution  
 68 chronostratigraphy (Table 1). Current metadata-rich databases that follow FAIR principles remain  
 69 limited to fewer than 3000  $\delta^{15}\text{N}$  entries (e.g., Farrell et al., 2021; Lai et al., 2025), highlighting the  
 70 urgent need for a rigorously standardized, spatiotemporally comprehensive  $\delta^{15}\text{N}$  database.



71  
 72 **Figure 1.** Temporal trends in (a) nitrogen isotope publications and (b)  $\delta^{15}\text{N}$  data entries in the DSMS-NI database.  
 73 Vertical bars denote annual publication/dataset counts, while dots connected by lines represent cumulative totals  
 74 over the years.  
 75

76 The DSMS-NI database, a repository of deep-time sediment nitrogen isotopes in marine systems  
 77 spanning Earth history, aims to address this need. The DSMS-NI database is a part of the broader  
 78 GBDB (Geobiology Database) project, which aims to build a comprehensive database of biotic and  
 79 biogeochemical evolution throughout time and to explore the mechanisms driving these evolutionary  
 80 processes. By integrating detailed metadata, DSMS-NI provides a valuable resource for studying  
 81 nitrogen cycle evolution and paleoenvironmental conditions at a range of temporal and spatial scales.  
 82 This compilation provides an extensive survey of  $\delta^{15}\text{N}$  records on bulk sediments and specific phases in  
 83 sediments deposited within marine environments, with a particular emphasis on data predating the

84 Cenozoic Era. Derived from 417 peer-reviewed publications and publicly available datasets, it  
 85 currently encompasses 70 854 discrete  $\delta^{15}\text{N}$  measurements for various components (e.g., bulk rock,  
 86 shell-bound, kerogen). In addition, it includes roughly 281 215 associated data points for carbon, sulfur  
 87 isotopes, and major and trace element concentrations reported alongside the  $\delta^{15}\text{N}$  values. Each entry is  
 88 linked to a comprehensive set of standardized metadata, ensuring consistency and facilitating robust  
 89 data analyses. Our goal is to make DSMS-NI a dynamic, evolving database that improves over time,  
 90 with data visualizations updated concurrently on the Geobiology Data website  
 91 (<https://geobiologydata.cug.edu.cn/>, last access: 30 April 2025).

92

93 **Table 1** Overview of deep-time  $\delta^{15}\text{N}$  compilation.

| Data Source                               | Number of Metadata |  | Spatial | Temporal range             |
|---|--------------------|--|---------|----------------------------|
|   |                    | $\delta^{15}\text{N}$ records  |         | range                      |
| Tesdal et al. (2013)                      | 33 352             | Fine age; Modern coordinate; Site  | Global  | Neogene to Present         |
| Algeo et al. (2014),<br>restricted access | 6006               | Broad age; Formation   | Global  | Ediacaran to Present       |
| Stüeken et al. (2016)                     | 6449               | Broad age; Formation; Lithology; Metamorphic grade   | Global  | Since the Paleoproterozoic |
| Stüeken et al. (2024)                     | 10 584             | Broad age; Formation; Lithology; Metamorphic grade   | Global  | Since the Eoarchean        |
| Kipp et al. (2018)                        | 6468               | Broad age; Formation; Lithology; Metamorphic grade   | Global  | Since the Paleoproterozoic |
| Koehler et al. (2019)                     | 2454               | Broad age; Formation; Lithology; Metamorphic grade   | Global  | Paleozoic                  |
| Farrell et al. (2021),<br>SGP database    | 840                | Broad age; Modern coordinate   | Global  | Paleozoic and Ediacaran    |
| Lai et al. (2025),<br>DM-SED database     | 2561               | Fine age; Modern coordinate; Paleocoordinate; Site; Formation; Depositional environments; Lithology; Metamorphic grade | Global  | Since the Neoproterozoic   |

94 *Note.* The classification of age resolution in the metadata is as follows:

95 - Broad age: Age estimates assigned uniformly to data from multiple stratigraphic levels within the

96 same geological formation, indicating no resolved internal chronological order.  
97 - Fine age: Sequentially ordered ages calculated for individual samples, derived from an established  
98 age-depth model.

99

100 Version 0.0.1 of the DSMS-NI database is available in CSV format on Zenodo  
101 (<https://doi.org/10.5281/zenodo.15117375>), and dynamic updates will be maintained on the  
102 GeoBiology website. The following sections provide a comprehensive overview of the database  
103 compilation methods, data structure, and details of the dataset, including data sources, selection criteria,  
104 and definitions of metadata fields. Additionally, we analyze the temporal and spatial trends of  $\delta^{15}\text{N}$   
105 within the dataset, discuss potential applications and limitations, and outline the foundation for the  
106 database's continuous development and scientific utility.

107 **2 Compilation methods**

108 **2.1 Data compilation**

109 An extensive search was conducted based on published articles, reports, theses, and datasets to gather  
110 all available literature on deep-time nitrogen isotopes. Initially, a keyword-based search combining  
111 geological period and nitrogen isotope was performed on Google Scholar, yielding over 3000 relevant  
112 literature sources after removing duplicates. A significant portion of the articles, however, only  
113 discussed previously published  $\delta^{15}\text{N}$  data, rather than presenting newly measured data, which were  
114 manually excluded from the data compilation. Additionally, geochemical databases such as PANGAEA  
115 (<https://www.pangaea.de/>, last access: April 1 2025), EarthChem (<https://www.earthchem.org/>, last  
116 access: April 1 2025), SGP (<https://sgp-search.io/>, last access: April 1 2025), and NOAA  
117 (<https://www.ncei.noaa.gov/>, last access: April 1 2025) were queried to ensure comprehensive coverage  
118 of dataset sources (Diepenbroek et al., 2002; Gard et al., 2019; Farrell et al., 2021). Where overlaps  
119 existed between datasets and publications, journal articles were prioritized as the primary data sources.  
120 Further filtering excluded studies on non-marine sediments, entries lacking essential metadata (e.g.,  
121 geological age, latitude and longitude), and a limited number of Cenozoic records with inaccessible  
122 data. Ultimately, the curated dataset includes 424 valid sources published between 1983 and 2024,  
123 representing a comprehensive compilation of nitrogen isotope records for deep-time marine sediments.

124 Data from each publication were stored in various formats, including tables within the main text,  
125 supplementary files, or shared databases. Data extracted from tables and supplementary files were

126 initially processed by computer algorithms, followed by manual verification and supplementation. For  
127 databases, data files were downloaded manually. In cases where publications did not provide direct  
128 data, data points were extracted from figures using GetData Graph Digitizer (ver. 2.24), and these  
129 entries were labeled as "plot" in the Notes section. Each publication was then organized into an  
130 individual data file with clear labeling of sources and unique site identifiers. These files were  
131 subsequently merged into a master dataset based on standardized column headers. In the final master  
132 dataset, additional metadata were curated, including geological age, latitude and longitude, lithology,  
133 depositional facies, and metamorphic grade. High-resolution ages and paleocoordinates were calculated  
134 and converted, where applicable.

135 **2.2 Data selection and quality control**

136 Given that biogeochemical and paleoenvironmental studies based on nitrogen isotopes require the  
137 assessment of the depositional environment and post-depositional alteration, geochemical data apart  
138 from  $\delta^{15}\text{N}$  are crucial (Tribouillard et al., 2006; Robinson et al., 2012). Therefore, we collected other  
139 contemporaneously published geochemical data of the same samples as  $\delta^{15}\text{N}$  from the literature  
140 relevant to the formations in our database. All available data from each research site were included as  
141 comprehensively as possible, rather than excluding entries solely due to the absence of  $\delta^{15}\text{N}$  values.  
142 This approach allows for the potential interpolation of the time-series data. However, geochemistry  
143 fields with fewer than 100 data points in the final compilation were excluded due to their limited  
144 analytical utility, such as Mo and Fe isotopes.

145 To ensure the reliability and applicability of the data, each entry underwent a rigorous screening  
146 and evaluation process. Initially, we assessed the data source and its spatiotemporal context. All studies  
147 included in the database were required to report verified  $\delta^{15}\text{N}$  values with clear data provenance and  
148 well-defined spatiotemporal information. Data entries lacking traceable sources were excluded.  
149 Similarly, entries without precise geographic or temporal information were not considered. Data from  
150 geological settings representing highly localized environments or with high metamorphic grades, such  
151 as samples affected by hydrothermal activity (Martin and Stüeken, 2024) or highly metamorphosed  
152 minerals (e.g., mica; Jia and Kerrich, 2000; Busigny et al., 2003), were also excluded given that their  
153  $\delta^{15}\text{N}$  compositions likely record alteration processes rather than seawater signatures. This filtering  
154 criterion was applied based on descriptions in the original literature rather than a fixed metamorphic  
155 grade threshold. The  $\delta^{15}\text{N}$  values for bulk rock and decarbonated rock were classified as primary entries  
156 ( $\delta^{15}\text{N}_{\text{bulk}}$ ), while values for specific phases, such as fossil shells, kerogen, clay-bound nitrogen, and

157 porphyrins, were categorized solely as secondary entries ( $\delta^{15}\text{N}_{\text{sp}}$ ). Only primary entries were analyzed  
158 in the data visualizations presented later in this study.

159 Only  $\delta^{15}\text{N}$  obtained through standardized, widely accepted techniques were included in the  
160 database. These primarily consist of elemental analyzer-isotope ratio mass spectrometry methods  
161 applied to bulk rock, decarbonated fractions, or kerogen (Song et al., 2023), as well as denitrifier-based  
162 mass spectrometry methods for microfossils (Ren et al., 2012; Smart et al., 2018). Studies employing  
163 non-standard or unvalidated methods, such as stepwise combustion (Ishida et al., 2017), were excluded.  
164 Data from highly metamorphosed settings (e.g., hydrothermal alteration), terrestrial lakes and rivers,  
165 modern organisms and their metabolic products, and liquid phases were flagged and omitted from the  
166 database (e.g., Bebout et al., 1999; Chase et al., 2019; Xia et al., 2022). For data from the same site but  
167 at different depths or lithologies, or for measurements of different components in the same layer (e.g.,  
168 bulk sediment and decarbonated sediment), or replicate analyses of the same homogenized sample,  
169 each entry was recorded separately to accurately capture variability.

170 Metadata on paleocoordinates, depositional setting, lithology, and metamorphic grade are  
171 included, wherever available. Entries were not excluded due to missing such metadata, as these can  
172 potentially be supplemented in future research. When such metadata were not directly reported in the  
173 literature, we attempted to estimate them using supplementary data or external sources, such as  
174 paleogeographic reconstructions. For entries for which metadata could not be determined, blank values  
175 were assigned.

### 176 **3 Data summary**

177 Since nitrogen isotope studies in sediments began in the late 1980s, the number of published studies  
178 has shown an accelerating growth trend, doubling approximately every decade. This trend is mirrored  
179 by a steady increase in data volume, with an average annual addition of around 2,720 data points over  
180 the past two decades (Fig. 1). However, the rate of data growth slightly lags behind that of publications,  
181 largely because early Ocean Drilling Program (ODP) and Integrated Ocean Drilling Program (IODP)  
182 projects contributed substantial datasets within individual publications (e.g., Liu et al., 2008). Ocean  
183 drilling remains a vital component of the database, covering geological intervals since the Cretaceous.  
184 Some early drilling data were not initially publicly accessible and have been supplemented through  
185 existing literature compilations, particularly the substantial dataset from Tesdal et al. (2013), along with  
186 enriched metadata.

187 The DSMS-NI database comprises a total of 31 metadata fields and 130 proxy data fields,  
188 organized into five primary categories (Table 2): (1) sampling location, (2) age information, (3)  
189 geochemical data, (4) lithological characteristics, (5) analytical methods and (6) references. For clarity  
190 and consistency throughout this data descriptor, the term "entries" refers to individual proxy values and  
191 their associated metadata (i.e., rows), while "fields" denote the metadata attributes recorded for each  
192 entry (i.e., columns).

193

194 **Table 2** Field names and descriptions.

| Field name                    | Description  |
|-------------------------------|--|
| Sample ID and location fields |  |
| SampleID                      | Unique sample identification code, as originally published   |
| SiteName                      | Name of the drill core site or section   |
| SampleName                    | Author denoted title for the sample (often non-unique, e.g., numbered)   |
| Location1                     | Detailed location of the data collection site  |
| Location2                     | Country or ocean of the data collection site   |
| Latitude                      | Modern latitude of collection site rounded to two decimals; negative values indicate the Southern Hemisphere (decimal degrees)     |
| Longitude                     | Modern longitude of the collection site rounded to two decimals; negative values indicate the Western Hemisphere (decimal degrees) |
| Paleolatitude                 | Paleolatitude of collection site rounded to two decimals; negative values indicate the Southern Hemisphere (decimal degrees)       |
| Paleolongitude                | Paleolongitude of the collection site rounded to two decimals; negative values indicate the Western Hemisphere (decimal degrees)   |
| Age fields                    |  |
| Era                           | The geologic era, in reference to GTS v202309  |
| Period                        | The geologic period, in reference to GTS v202309   |
| Epoch                         | The geologic epoch, in reference to GTS v202309  |
| Stage                         | The geologic stage, in reference to GTS v202309  |
| Age                           | Age, in reference to GTS v202309   |
| Formation                     | Geologic formation name  |
| Unit                          | Specific geologic event layers   |

|                                    |  |
|------------------------------------|--|
| RelativeDepth                      | Stratigraphic height or depth (m)  |
| Petrological characteristic fields |  |
| Lithology                          | Lithological name of the sample, as originally published   |
| LithType                           | Lithology type of sample (e.g., carbonate, siliciclastic)  |
| MetamorphicGrade                   | The degree to which the rock has undergone transformation due to heat and pressure conditions  |
| Setting                            | Depositional environment (e.g., epeiric, bathyal)  |
| WaterDepth                         | Estimated depositional water depth of the data collection site   |
| Method fields                      |  |
| Material                           | Samples subjected to $\delta^{15}\text{N}$ analysis (e.g., decarbonated sediment, diatom, kerogen)   |
| Technique $\delta^{15}\text{N}$    | Methodology employed for $\delta^{15}\text{N}$ measurement (e.g., EA combustion, denitrifier method)   |
| Data fields                        |  |
| Isotopes                           | The isotopic composition expressed in per mille (‰) as $\delta$ (e.g., $\delta^{15}\text{N}$ , $\delta^{13}\text{C}$ )                       |
| Elements                           | The concentration of elements within rocks (e.g., TN, P, Fe, Cu, Ce)   |
| RockEval                           | Proxies of hydrocarbon potential measured by pyrolysis method (e.g., S1, OI, $T_{\max}$ )  |
| FeSpecies                          | Concentrations and ratios of different iron species in rocks (e.g., $\text{Fe}_{\text{py}}$ , $\text{Fe}_{\text{HR}}/\text{Fe}_{\text{T}}$ ) |
| Reference fields                   |  |
| FirstAuthor                        | The last name of the first author of the original publication  |
| Year                               | The year of the original publication   |
| Title                              | The title of the original publication  |
| Reference                          | The formatted reference of the original publication  |
| DOI                                | The DOI of the original publication  |
| DataSource                         | The repository hosting the data except for the original publication  |

195

196        **Sample ID and Location fields.** Each data entry was assigned a unique Sample ID to distinguish  
 197        it from other data entries. Geographic location information includes the modern latitude and longitude  
 198        (Latitude and Longitude) referencing WGS84 (World Geodetic System 1984), obtained directly from

199 original literature or external sources whenever possible. For studies that do not provide exact  
200 coordinates, approximate locations are estimated based on geographic descriptions or accompanying  
201 maps, using tools such as Google Maps. Additionally, we record the broader sampling region (e.g.,  
202 country or oceanic region) and specific sampling site details (such as province, county, or uplift names).  
203 The location fields also include the name of the drilling site or outcrop section (SiteName), which  
204 identifies the precise drilling location or outcrop at which samples were collected, providing valuable  
205 geographic context. Certain SiteNames are uniquely associated with major drilling projects (e.g., ODP,  
206 IODP), which is important for subsequent data supplementation and analysis. Some samples also have  
207 a SampleName, as designated by the original authors—typically a code or non-unique label reflecting  
208 the naming format in the primary literature. Although multiple samples in the database may share the  
209 same SampleName, each entry has a distinct Sample ID to ensure the uniqueness of each record.

210 We also provide paleolatitude and paleolongitude (PaleoLatitude and PaleoLongitude), calculated  
211 based on the geological age of each sample and using paleogeographic reconstruction tools such as  
212 PointTracker v7.0, built on the plate rotation model of Scotese and Wright (2018). Paleocoordinate data  
213 are crucial for understanding the historical shifts in sample locations and their relationship to  
214 depositional environments (Percival et al., 2022; Li et al., 2025). To maintain consistency, all  
215 geographic coordinates are standardized to two decimal places.

216 **Age fields.** Each entry includes not only absolute age data but also a series of geologic age-related  
217 fields to provide precise temporal context. These fields enable targeted data retrieval at a range of  
218 geological timescales, facilitating comparisons with newly added data. The GeologicalAge field  
219 captures broad temporal frameworks, recorded as Epoch for the Phanerozoic (e.g., Early Triassic) and  
220 Era for the Precambrian (e.g., Neoproterozoic). For more refined stratigraphic resolution, the Stage  
221 field (e.g., Induan) is used, with the System as a substitute for Precambrian samples (e.g., Ediacaran).  
222 The Age field records the absolute age of each sample, following the International Chronostratigraphic  
223 Chart, GTS v202309. The Formation field notes the geological unit (formation or member) from which  
224 the sample was collected, aiding in understanding its depositional context and relation to surrounding  
225 strata (Murphy and Salvador, 1999). However, Formation data are generally limited to outcrop sections,  
226 as ocean drilling samples lack specific formation designations. The Unit field identifies particular  
227 stratigraphic units or geologic event layers, such as the Cretaceous pre-OAE2 or OAE2 (Jenkyns,  
228 2010), which aids in correlating samples within recognized geological events. The RelativeDepth field  
229 records the sample's relative depth in the section or drill core, which is essential for high-resolution age

230 analyses and sedimentation rate calculations.

231 Age data allocation follows these guidelines below. When precise ages and geological age  
232 information for each sample were provided in the original source, these values are prioritized. However,  
233 for data from the Common Era (i.e., negative ages), they are uniformly assigned a value of 0 Ma,  
234 meaning that all such data are treated as reference values for modern top sediments. Otherwise, age  
235 assignments follow two methods based on data availability. (1) For records with at least two samples or  
236 stratigraphic horizons of known age (e.g., radiometrically dated layers or well-defined stage  
237 boundaries), we constructed an age-depth model. This model linearly interpolates ages between these  
238 tie-points along the RelativeDepth axis, assuming a constant sedimentation rate within each interval  
239 between stratigraphic age tie-points. While this assumption is effective for establishing the relative  
240 temporal sequence of samples, which is critical for capturing first-order stratigraphic trends, it  
241 necessarily introduces uncertainties in absolute age determination due to potential variability in  
242 sedimentation rates or local stratigraphic features. (2) For records lacking sufficient data for an  
243 age-depth model, a single age was assigned to all samples. When only one age constraint (e.g., a  
244 radiometric date from a nearby stratum) is available, that specific age is applied. In the absence of any  
245 direct age control, the median age of the corresponding geologic stage is used as a default. It should be  
246 noted that assigning a uniform age to a suite of samples, particularly using the median stage age, carries  
247 significant uncertainty, theoretically on the order of the duration of the entire geologic interval (which  
248 can approach 100 Myr for long stages of the Precambrian). Profiles constrained by a single radiometric  
249 date, which is the predominant method for dating sequences older than 600 Ma, are generally more  
250 reliable than those relying solely on a median stage age.

251 **Data fields.** The dataset includes analyses of isotopic compositions, elemental concentrations, and  
252 specific components. To maintain consistency, all units were standardized during data collection, as  
253 original publications sometimes report these data in varying units. (1) Isotopic data include  $\delta^{15}\text{N}$ ,  $\delta^{13}\text{C}$ ,  
254  $\delta^{18}\text{O}$ , and  $\delta^{34}\text{S}$ , all expressed in ‰ relative to international standards. Nitrogen isotopes are reported  
255 relative to atmospheric nitrogen (Air  $\text{N}_2$ ), carbon and oxygen isotopes relative to the Vienna Pee Dee  
256 Belemnite (VPDB) standard, and sulfur isotopes relative to the Vienna Canyon Diablo Troilite (VCDT)  
257 standard (Hoefs, 2009). (2) Elemental concentrations include TN (total nitrogen), TOC (total organic  
258 carbon), TS (total sulfur),  $\text{CaCO}_3$ , TC (total carbon), TIC (total inorganic carbon), P, Al, K, Si, Ca, Ti,  
259 Na, Mg, Fe, as well as iron species data and LOI (loss-on-ignition), and they are reported in weight  
260 percent (wt %). Concentrations of other trace elements are standardized to parts per million (ppm). (3)

261 Some data originally reported as oxide concentrations were converted to elemental concentrations  
262 based on stoichiometric ratios, such as P<sub>2</sub>O<sub>5</sub>. (4) Additional derived values include ratios of iron species,  
263 dry bulk density, and rock eval indices (Peters et al., 1986; Poulton and Canfield, 2005). These indices  
264 comprise alkenone content (C37, in nmol/g), oxygen index (OI, mg CO<sub>2</sub>/g TOC), hydrogen index (HI,  
265 mg HC/g TOC), maximum pyrolysis temperature (T<sub>max</sub>, °C), free hydrocarbons (S1, mg HC/g Rock),  
266 hydrocarbons generated from rock pyrolysis (S2, mg HC/g Rock), and CO<sub>2</sub> released from organic  
267 matter pyrolysis (S3, mg CO<sub>2</sub>/g Rock). Some inaccessible data points were visually extracted from  
268 figures using scatterplot recognition techniques, which are marked as "plot" in the Notes field. Data  
269 with values exceeding detection limits or those erroneous (e.g., negative values for element  
270 concentration) were excluded from the dataset.

271 **Petrological characteristic field.** The petrological characteristic fields encompass information on  
272 lithology, depositional facies, and metamorphic grade, which provide essential contextual support for  
273 subsequent isotopic geochemistry analyses. (1) Lithology: The Lithology field records the original  
274 descriptions provided by authors, using terms such as "black shale" "mudstone" "limestone" and  
275 "breccia". The LithType field classifies these lithologies into broader categories, primarily as carbonate  
276 and siliciclastic (Tucker and Wright, 2009), with minor entries for phosphorite and iron formations. (2)  
277 Metamorphic Grade: The metamorphic grade field reflects the extent of metamorphism the samples  
278 have undergone, based on original terminology whenever possible. Common terms include specific  
279 metamorphic facies (e.g., amphibolite, greenschist) as well as general descriptors like  
280 "unmetamorphosed" and "low grade". For Cenozoic samples, which are generally assumed to have  
281 undergone minimal metamorphic alteration (Winter, 2014), any entries lacking detailed descriptions are  
282 uniformly designated as "unmetamorphosed". (3) Depositional Setting: This field records the  
283 depositional environment of each sample, with terms like "neritic" "peritidal" "slope" and "abyssal"  
284 preserved from the original literature. For many ocean drilling samples, depositional settings are  
285 inferred from WaterDepth: depths of 500–2000 m are classified as "bathyal" and depths exceeding  
286 2000 m are designated as "abyssal".

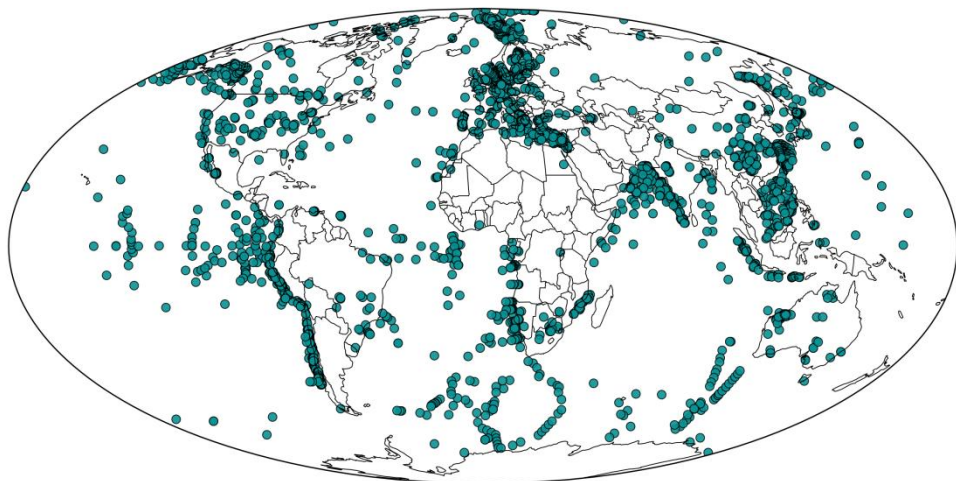
287 **Data collection sources.** Data in the database primarily originate from published literature and  
288 are traceable via DOI. Some data come from public databases such as PANGAEA, SGP, and NOAA.  
289 Each record includes multiple fields for source information, such as first author, publication year,  
290 article title, reference, DOI, and data source. Metadata fields have been standardized and cleaned via  
291 code to ensure consistency and machine readability, removing special characters while retaining

292 complete citation formats. This structure allows users to trace data provenance, with DOI or Reference  
293 fields facilitating direct searches on Crossref for verification.

294 **4 Technical validation**

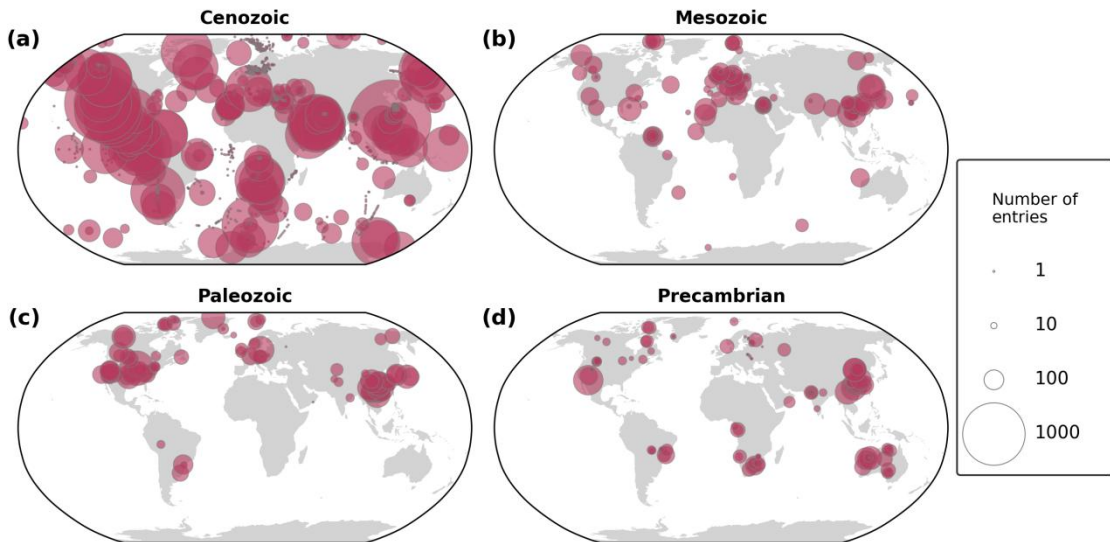
295 The DSMS-NI database has undergone meticulous curation and quality control (QC) to ensure data  
296 accuracy, consistency, and scientific value. Each record includes comprehensive metadata to support  
297 traceability and verification. While each entry and significant metadata contain a simple remarks field  
298 (excluded from the main database to prevent clutter), it notes the source or reason for inclusion,  
299 facilitating validation and cross-checking by the data management team. We implemented several QC  
300 measures to verify database accuracy.

301 **Geographic coordinate verification.** Latitude and longitude values were checked to confirm  
302 they fall within the valid ranges of  $-90$  to  $90$  and  $-180$  to  $180$ , respectively. Sample coordinates were  
303 cross-referenced with country names and public national boundaries to ensure geographic accuracy.  
304 Modern sample coordinates were projected onto a global map with administrative boundaries (Figs. 2-3)  
305 to verify logical placements. If coordinates appeared on land or in other unexpected locations, each  
306 entry was manually reviewed and corrected as needed.



307

308 **Figure 2.** Distribution of sample sites on modern global map.



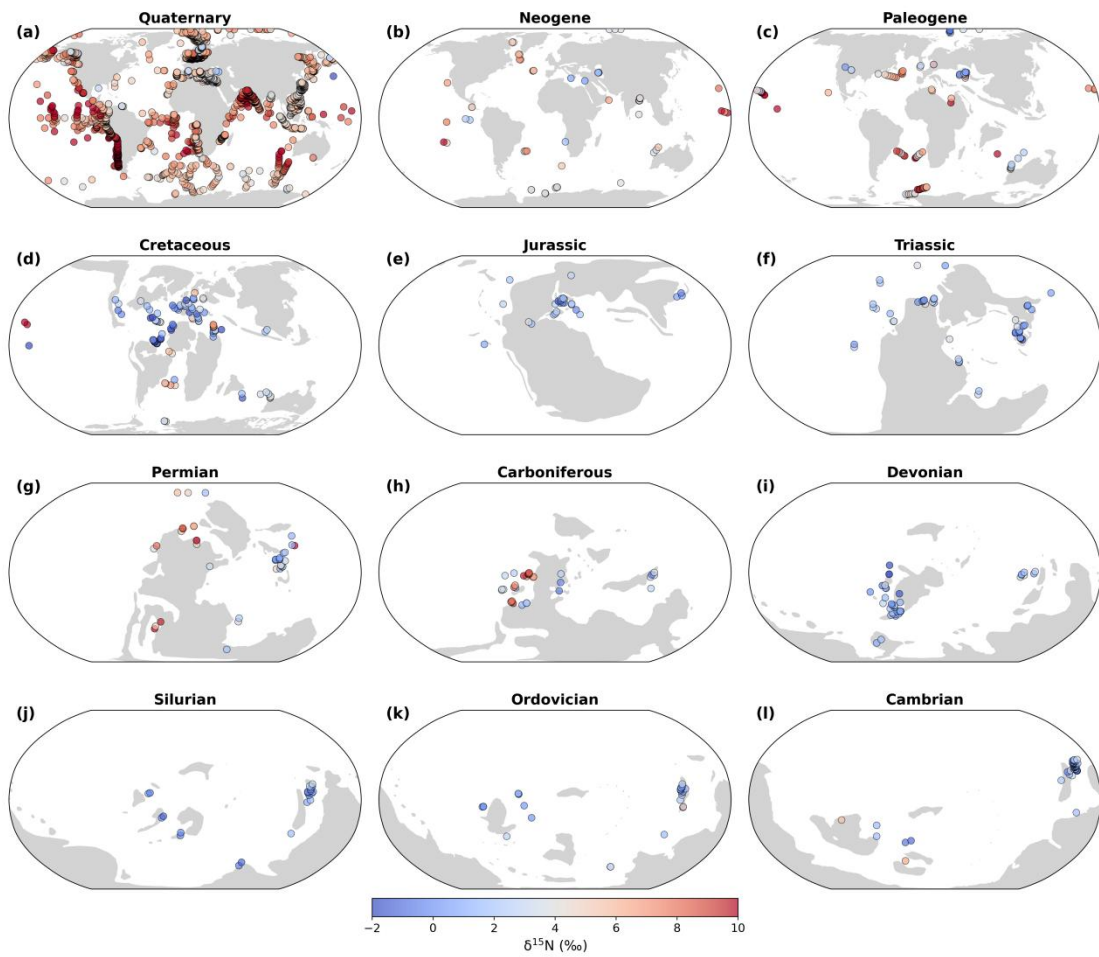
309

310 **Figure 3.** Spatial distribution of sampling sites and sample quantities by geological era in a modern geographic  
 311 reference frame. The base map is adapted from Kocsis and Scotese (2021). The term "entries" refers to individual  
 312 proxy values and their associated metadata (i.e., rows in the DSMS-NI database).

313

314 **Paleocoordinate validation.** Paleolatitudes and paleolongitudes were calculated using the  
 315 G-Plates model (Scotese and Wright, 2018) and PointTracker v7.0 software, ensuring alignment with  
 316 each sample's geological age and geographical context. Site locations were plotted on paleogeographic  
 317 maps (Fig. 4) for further evaluation; any inconsistencies in paleocoordinates were flagged, reviewed,  
 318 and adjusted accordingly.

319 **Outlier detection.** Frequency histograms and time-series scatter plots were generated to identify  
 320 potential outliers in the dataset. All flagged extreme values underwent secondary validation against  
 321 their original sources to confirm the accuracy. This process led to the correction of erroneous entries  
 322 introduced during unit conversions and the removal of invalid data points that fell outside instrumental  
 323 detection limits. Extreme  $\delta^{15}\text{N}$  values falling outside a conservative range ( $< -10\text{‰}$  or  $> +40\text{‰}$ ) were  
 324 excluded from the final compilation (e.g., Thomazo et al., 2011; Hammarlund et al., 2019). This  
 325 decision was based not on the validity of the individual measurements, but on the need to prioritize  
 326 data representativeness for global-scale analysis. The excluded values, even if explained within their  
 327 original publication context, are statistical outliers that have not been corroborated and could unduly  
 328 influence broad interpretations.



329

330 **Figure 4.** Paleogeographic distribution of  $\delta^{15}\text{N}$  values by geological period. The base map is adapted from Kocsis  
331 and Scotese (2021).

332

333 **Duplicate check.** We conducted a comprehensive check for duplicate entries, especially for  
334 samples with similar GPS coordinates. All suspected duplicates were carefully compared, and  
335 necessary corrections were made to eliminate redundancy.

336 **Age model calibration.** To minimize errors, geological age data were entered using a  
337 standardized template to prevent typos, inconsistencies, or incorrect values. Automated analyses and  
338 cross-verification ensured that numerical ages corresponded accurately with designated eras and  
339 geological stages. A mismatch between a numerical age and its geological stage often indicates an  
340 outdated age in the original reference (e.g., Wang et al., 2013). To address this, we recalibrated the  
341 outdated estimations by building new age-depth models based on the current geologic stage boundaries  
342 from the International Chronostratigraphic Chart (GTS v202309).

343 **Data collection sources.** Citation information within the reference field was obtained through  
344 automated methods from the CrossRef platform, ensuring uniformity in citation formatting (Hendricks  
345 et al., 2020). We used scripts to extract comprehensive bibliographic details for each publication,

346 including author names, title, publication year, journal name, volume, page numbers, and DOI. This  
347 automation significantly reduced potential spelling errors and inconsistencies that may arise in manual  
348 entry. Extracted citation data were cross-checked against original entries in the database, and any  
349 discrepancies or errors were corrected manually by the data management team to maintain source  
350 accuracy and completeness.

351 **5 General database statistics**

352 The latest version of the DSMS-NI database comprises approximately 320 000 data entries, including  
353 70 854  $\delta^{15}\text{N}$  records, spanning all geological periods from the Eoarchean (~3800 Ma) onward. These  
354 records originate from a diverse array of unique sampling sites, encompassing ocean drilling cores and  
355 outcrop sections. The  $\delta^{15}\text{N}$  data are predominantly concentrated in the Phanerozoic, comprising 92.1 %  
356 of the total database, with further breakdowns showing 71.7 % in the Cenozoic, 8.3 % in the Mesozoic,  
357 and 12.1 % in the Paleozoic (Table 3 and Fig. 3). The following sections focus on first-order spatial and  
358 temporal trends in  $\delta^{15}\text{N}$  data density, sampling locations, and values within DSMS-NI. The provided  
359 figures illustrate only a subset of the spatial-temporal patterns uniquely revealed by this extensive  
360 compilation, demonstrating the database's potential to advance research in paleoclimate, geochemistry,  
361 and paleoecology.

362

363 **Table 3** The quantities and proportions for  $\delta^{15}\text{N}$ ,  $\delta^{13}\text{C}_{\text{org}}$ , TN, and TOC of each geological era.

| Proxy system                       | Cenozoic | Mesozoic | Paleozoic | Precambrian | Total  |
|------------------------------------|----------|----------|-----------|-------------|--------|
| $\delta^{15}\text{N}$              | 50 795   | 5877     | 8555      | 5625        | 70 852 |
|                                    | 71.7 %   | 8.3 %    | 12.1 %    | 7.9 %       |        |
| $\delta^{13}\text{C}_{\text{org}}$ | 10 783   | 4882     | 6873      | 4494        | 270 32 |
|                                    | 39.9 %   | 18.1 %   | 25.4 %    | 16.6 %      |        |
| TN                                 | 31 530   | 2852     | 6441      | 4977        | 45 800 |
|                                    | 68.8 %   | 6.2 %    | 14.1 %    | 10.9 %      |        |
| TOC                                | 22 615   | 5059     | 8555      | 5118        | 41 347 |
|                                    | 54.7 %   | 12.2 %   | 20.7 %    | 12.4 %      |        |

364

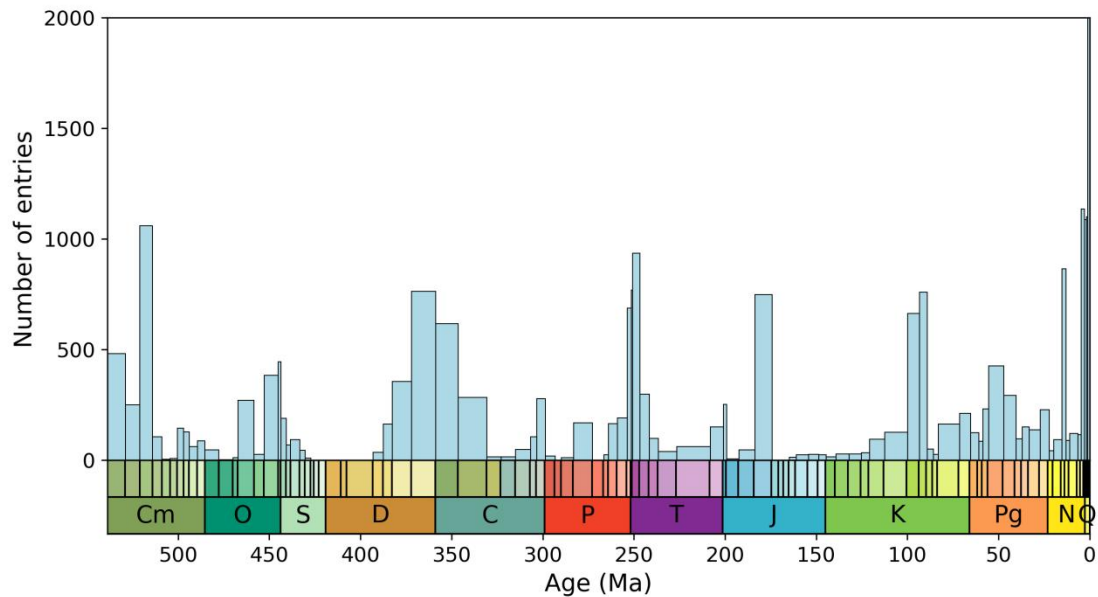
365

366

367 **5.1 Temporal density and evolution of  $\delta^{15}\text{N}$** 

368 Given that the data are concentrated in the Phanerozoic, for which ages are more precisely constrained,  
 369 we performed a detailed stratigraphic breakdown of age distribution by stage within the Phanerozoic  
 370 (Fig. 5). The distribution is uneven, with the highest data densities in recent periods, particularly the  
 371 Holocene (0–12 ka), Late Pleistocene (12–129 ka), and Chibanian (129–770 ka). The high data density  
 372 in the Quaternary primarily reflects the abundance of high-resolution records from various ocean  
 373 drilling projects, whose individual cores contributed large and densely sampled datasets. In contrast,  
 374 older geological periods exhibit data clusters around key events, such as biotic radiations, mass  
 375 extinctions, and oceanic anoxic events (Bush and Payne, 2021). Notable gaps or low-density intervals  
 376 occur in the mid-Cambrian to Early Ordovician, Silurian to Early Devonian, mid-Carboniferous to  
 377 Early Permian, mid-Triassic to Early Jurassic, and Late Jurassic to Early Cretaceous.

378



379

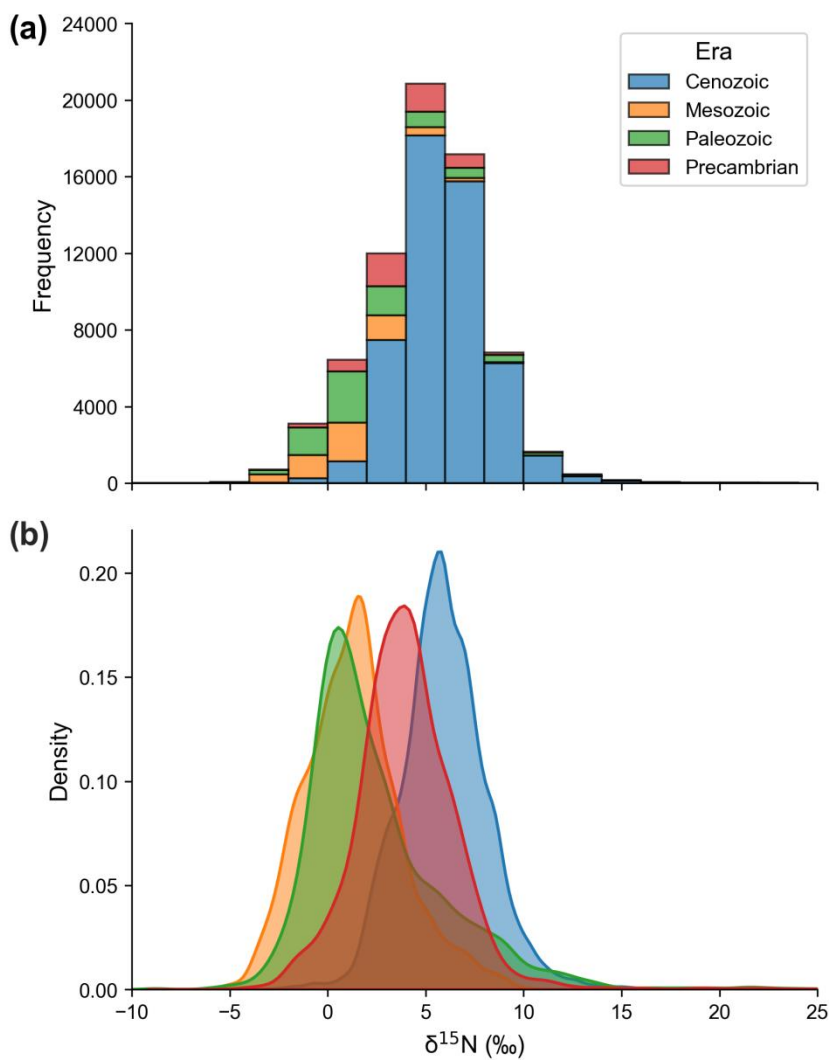
380 **Figure 5.** Number of data points binned by geologic stage. Data counts for the Holocene (0–12 ka), Late  
 381 Pleistocene (12–129 ka), and Chibanian (129–770 ka) stages are 10 640, 21 754, and 8378, respectively; these  
 382 counts are not displayed in the figure due to narrow column width. The Precambrian has only 5646 data points,  
 383 accounting for 7.9%, and is not shown. Cm: Cambrian; O: Ordovician; S: Silurian; D: Devonian; C: Carboniferous;  
 384 P: Permian; T: Triassic; J: Jurassic; K: Cretaceous; Pg: Paleogene; N: Neogene; Q: Quaternary.

385

386 Overall,  $\delta^{15}\text{N}$  values exhibit a unimodal distribution centered around +5 ‰, with a mean of  $5.1 \pm$   
 387 9.1 ‰ ( $1\sigma$ ; Fig. 6a). When examining the modal values of the era-specific kernel density distributions,  
 388 the Cenozoic exhibits the highest mode, followed by the Precambrian, with significantly lower modal

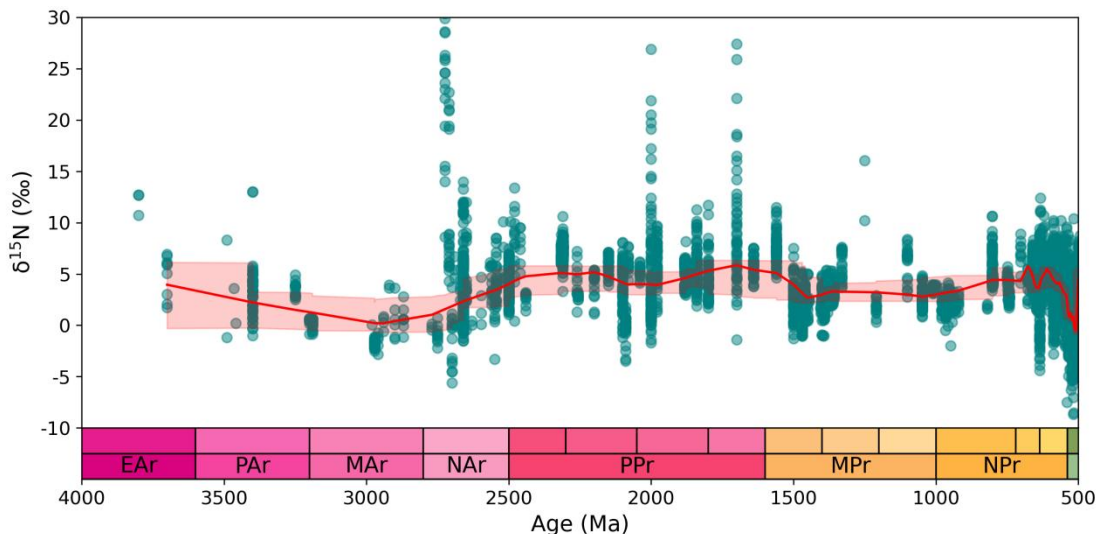
389 densities in the Paleozoic and Mesozoic (Fig. 6b). The Precambrian data, which have a dispersed  
 390 distribution (Fig. 7), indicate an unstable nitrogen cycle, a state potentially driven by the evolution of  
 391 microbial metabolisms and later overprinted by metamorphism (see Ader et al., 2016; Stüeken et al.,  
 392 2024 for further discussion). LOWESS smoothing results reveal  $\delta^{15}\text{N}$  peaks in the Neoarchean,  
 393 Paleoproterozoic, and Ediacaran, i.e., periods closely associated with significant oxygenation events  
 394 (Kipp et al., 2018; Koehler et al., 2019; Pellerin et al., 2024).

395



396

397 **Figure 6.** (a) Histogram and (b) density distribution of all  $\delta^{15}\text{N}$  data ( $n = 69\,697$ ).



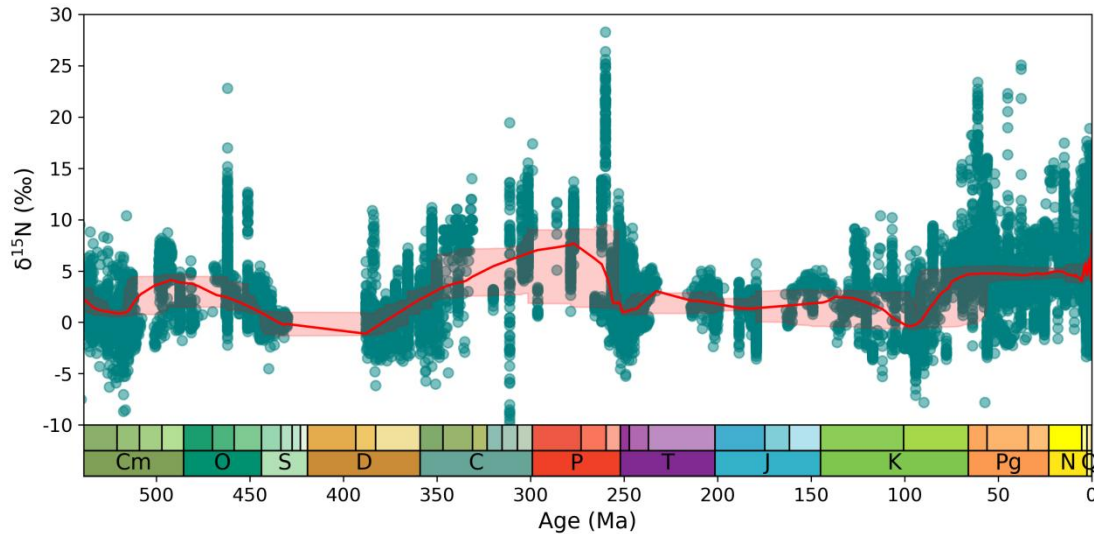
398

399 **Figure 7.**  $\delta^{15}\text{N}$  data and LOWESS curve through Precambrian. A LOWESS factor of 0.01 and a confidence  
400 interval of 2.5–97.5 % were applied. EAr: Eoarchean; PAr: Paleoarchean; MAr: Mesoarchean; NAr: Neoarchean;  
401 PPr: Paleoproterozoic; MPr: Mesoproterozoic; NPr: Neoproterozoic.

402

403 An examination of  $\delta^{15}\text{N}$  record reveals first-order variations on multi-million-year timescales  
404 since the Cryogenian. The LOWESS curve shows extended intervals of relatively elevated  $\delta^{15}\text{N}$  ( $>$   
405 +5 ‰) during the Cambrian/Ordovician transition, the Carboniferous–Permian, and the late  
406 Cretaceous–Cenozoic (Fig. 7). These broad peaks are separated by periods of lower  $\delta^{15}\text{N}$  values during  
407 the Ediacaran–Cambrian, Ordovician–Devonian, and Triassic–Cretaceous. The prolonged intervals  
408 (except for the Cambrian/Ordovician transition) of elevated  $\delta^{15}\text{N}$  broadly coincide with known periods  
409 of sustained cool climates or major glaciations (i.e., the Sturtian–Marinoan glaciations, the Late  
410 Paleozoic Ice Age, and the Cenozoic Icehouse), whereas the low  $\delta^{15}\text{N}$  intervals generally align with  
411 warmer greenhouse periods (i.e., most of the late Ediacaran–early Carboniferous and the Mesozoic)  
412 (Montañez et al., 2011; Macdonald et al., 2019). This tectonic-scale pattern mirrors observations from  
413 orbital-scale glacial-interglacial cycles (Ren et al., 2017) and transient hyperthermal events like the  
414 Paleocene/Eocene Thermal Maximum (Junium et al., 2018), suggesting that climate exerts a first-order  
415 influence on the marine nitrogen cycle. The underlying mechanisms may involve variations in ice sheet  
416 extent and sea level, which affect the distribution of oxygen-minimum zones (OMZs) and the  
417 proportion of water-column denitrification versus sedimentary denitrification (Algeo et al., 2014; Wang  
418 et al., 2022). However, the correlation is not straightforward; for instance, the increase in  $\delta^{15}\text{N}$  began in  
419 the Late Cretaceous, coinciding with the onset of global cooling but preceding the major expansion of  
420 Antarctic ice sheets in the Cenozoic (Judd et al., 2024). Therefore, the exact mechanisms coupling

421 climate and nitrogen cycle evolution remain an unsolved question for future research, ideally  
422 integrating Earth system models with the spatial  $\delta^{15}\text{N}$  data presented here.

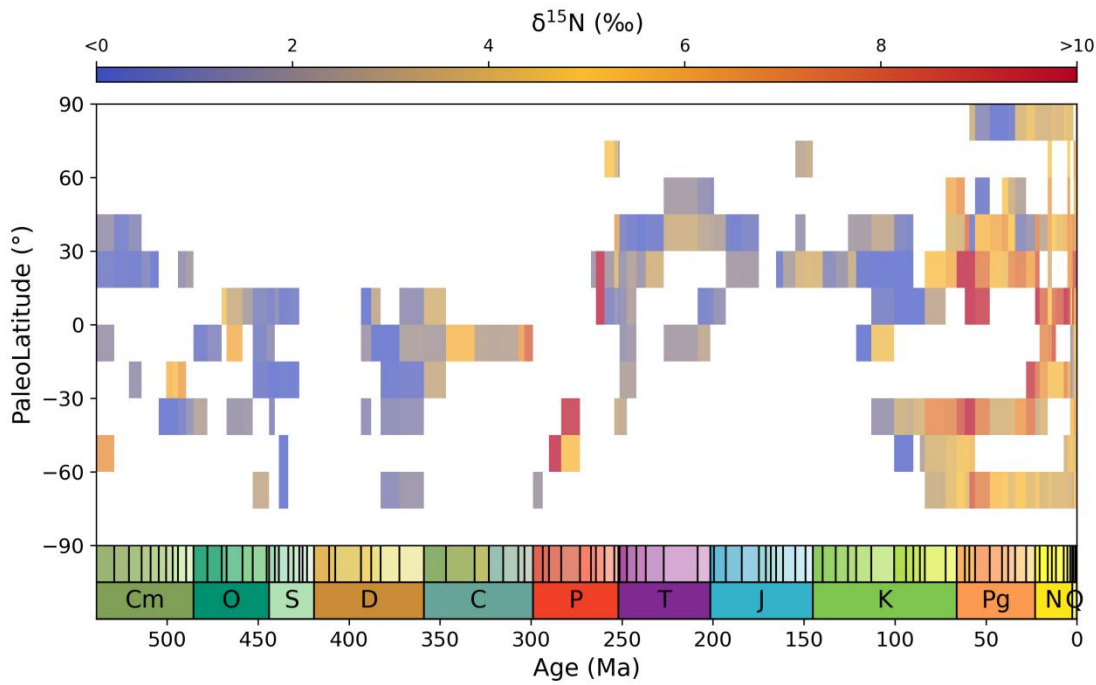


423  
424 **Figure 8.**  $\delta^{15}\text{N}$  data and LOWESS curve through the Phanerozoic. A LOWESS factor of 0.03 and a confidence  
425 interval of 2.5–97.5 % were applied.

426

427 **5.2 Spatial density and characteristics of  $\delta^{15}\text{N}$**

428 Spatial trends in data density within the DSMS-NI database reveal substantial variability in both  
429 modern (Fig. 2) and paleogeographic distributions (Fig. 4). Ocean drilling sites are primarily  
430 concentrated along continental margins and deep-sea basins, with significant gaps in central oceanic  
431 regions (National Research Council, 2011). For older strata (pre-Cretaceous), sampling sites are  
432 clustered in North America, Europe, China, and South Africa (Fig. 2). In terms of latitude,  $\delta^{15}\text{N}$   
433 sampling in older strata is sparse in the modern equatorial region and the mid- to high-latitude areas of  
434 the Southern Hemisphere, aside from some Southern Hemisphere samples collected from Cenozoic  
435 ocean drilling sites (Fig. 3). When modern coordinates are converted to paleolatitudes and mapped onto  
436 paleogeographic reconstructions, the Cenozoic Era provides the most extensive latitudinal coverage,  
437 with the Quaternary period contributing the highest number of sites, followed by the Cretaceous (Figs.  
438 4 and 9). In terms of marine spatial distribution,  $\delta^{15}\text{N}$  data since the Cretaceous reflects global patterns  
439 to a certain degree (Fig. 4). However, pre-Jurassic data remain spatially concentrated, with Paleozoic  
440 sites limited to just two or three main areas. High-latitude sampling is generally scarce, with Paleozoic  
441 sites predominantly in the Southern Hemisphere and Mesozoic sites mainly in the Northern  
442 Hemisphere (Fig. 4).



443

444 **Figure 9.** Spatio-temporal trends in  $\delta^{15}\text{N}$  values through the Phanerozoic, binned and averaged temporally by stage  
445 and spatially by  $15^\circ$  paleolatitudinal bins.

446

447 To visualize spatial trends, average  $\delta^{15}\text{N}$  values from each Phanerozoic period were mapped onto  
448 paleogeographic reconstructions for the respective period (Fig. 4). Significant spatial differences exist  
449 in  $\delta^{15}\text{N}$  distribution for different geological periods. In modern ocean sediments, elevated  $\delta^{15}\text{N}$  values  
450 (notably  $> +5\text{ ‰}$ ) are concentrated in regions influenced by upwelling, such as the Arabian Sea,  
451 southeastern Indian Ocean, eastern equatorial Pacific, southwestern South America, and the western  
452 coast of Mexico (Fig. 4a; Tesdal et al., 2013; Du et al., 2005b). In contrast, lower  $\delta^{15}\text{N}$  values  
453 (significantly  $< +5\text{ ‰}$ ) are typically found in restricted basins or broad continental shelves, such as the  
454 Black Sea, the Mediterranean Sea, the Baltic Sea, and the South China Sea. The global mean  $\delta^{15}\text{N}$   
455 (approximately  $+5\text{ ‰}$ , as observed in open ocean like the Southern Ocean) lies between these extremes.  
456 The modern spatial distribution of  $\delta^{15}\text{N}$  can provide a valuable framework for interpreting past marine  
457 conditions, as  $\delta^{15}\text{N}$  serves as an indicator of nutrient supply, upwelling intensity, and the extent of  
458 oceanic oxygen minimum zones (Altabet et al., 1999; Godfrey et al., 2025). However, analyzing spatial  
459 patterns in deep-time  $\delta^{15}\text{N}$  records is inherently limited by the scarcity of data, particularly from  
460 open-ocean settings, making it difficult to estimate global mean values and relative spatial gradients.  
461 For the Paleogene and Neogene,  $\delta^{15}\text{N}$  values were generally higher in the open ocean than in  
462 continental margin and restricted basins (Fig. 4b-c). In the Paleozoic and Mesozoic,  $\delta^{15}\text{N}$  values are  
463 generally negative, lacking prominent hotspots except in the Carboniferous and Permian. This pattern

464 may reflect a systematic bias, as available data are predominantly derived from continental shelf  
465 environments (Judd et al., 2020), which tend to exhibit lower  $\delta^{15}\text{N}$  values compared to the open ocean.  
466 Despite differences in paleogeographic position and absolute  $\delta^{15}\text{N}$  values, rapid shifts in  $\delta^{15}\text{N}$  exhibit  
467 consistent directional changes (increase or decrease) during key Phanerozoic transition events, such as  
468 the Permian-Triassic boundary (Knies et al., 2013; Du et al., 2021, 2023) and the Late Cretaceous  
469 (Meyers et al., 2009; Junium et al., 2018; Du et al., 2025b). Given the current uneven distribution of  
470 sampling sites, further  $\delta^{15}\text{N}$  studies of multiple regions are crucial for enhancing our understanding of  
471 the spatial characteristics of nitrogen cycle evolution in deep time.

472 **6 Usage notes**

473 **6.1 Informed user notice**

474 Each record (row) in the database includes detailed temporal and spatial metadata, along with lithology,  
475 metamorphic grade, and depositional facies information, where available. These metadata are essential  
476 for evaluating the geological context and fidelity of nitrogen isotope data. However, this version of the  
477 database has certain limitations: it may not capture all possible geological age uncertainties or precise  
478 depositional environment details for some records; significant gaps remain in the compilation of data  
479 for certain materials and time intervals (e.g. Quaternary). Consequently, users may need to  
480 independently assess and refine the metadata (e.g., chronological constraints) and supplement missing  
481 data (e.g., coral-bound  $\delta^{15}\text{N}$  records) as necessary for their specific applications. Despite our extensive  
482 efforts to accurately identify and quality-control each entry, given the vast dataset, some overlooked  
483 errors or data inconsistencies may remain. Users are encouraged to report any issues or omissions to  
484 the authors, as corrections will be incorporated into future database versions. We plan to release a new  
485 version of the dataset annually on Zenodo and update it on the Geobiology Database website. Each  
486 version will incorporate corrections to identified errors and integrate newly published data from the  
487 previous year to the fullest extent possible. This systematic update cycle is designed to ensure the  
488 dataset's accuracy, relevance, and long-term value for the research community.

489 In addition to  $\delta^{15}\text{N}$  data, the database provides geochemical information such as TOC, total TN,  
490  $\delta^{13}\text{C}_{\text{org}}$ , and major and trace element concentrations. These supplementary data are valuable for  
491 assessing factors that may influence nitrogen isotopes, such as organic matter preservation and redox  
492 conditions. Even when not directly paired with  $\delta^{15}\text{N}$  values, we retain all relevant data to enable users  
493 to conduct correlation analyses via interpolation or other methods. Researchers are welcome to

494 contribute additional geochemical data from the same sites or samples as they become available,  
495 allowing for updates and refinements in subsequent database releases.

496 **6.2 Applying the database to deep-time studies**

497 When applying the database to deep-time studies, certain filtering criteria can be used. For instance,  
498 samples may be selected based on lithology, metamorphic grade, and other metadata to ensure that the  
499 data aligns with specific geological research contexts. Temporal, paleolatitude, and paleodepth  
500 information are critical for paleogeographic reconstructions and spatiotemporal distribution analyses,  
501 particularly when investigating paleoclimate change and global biogeochemical cycles. Further  
502 analysis of variations in latitude, basin characteristics, and water depth has the potential to yield  
503 significant insights. Given the rapid variability of nitrogen isotopes and their pronounced regional  
504 characteristics, filling temporal and spatial gaps and enhancing resolution are of great  
505 value—particularly for pivotal periods like the Ordovician-Silurian mass extinction, the Early  
506 Devonian terrestrial plant radiation, and the Late Jurassic-Early Cretaceous supercontinent breakup.  
507 The database is also especially suited for comparative studies of key geological periods, such as the  
508 Permian-Triassic boundary extinction and the Cretaceous OAE2. Given the inherent limitations of our  
509 simplified age-depth models, we recommend that users seeking higher chronological precision for  
510 time-series analysis incorporate additional stratigraphic constraints (e.g., paleomagnetic or  
511 cyclostratigraphic data) to develop finer-scale age models, where necessary. To support these  
512 applications, we have also provided a software tool on Zenodo, allowing users to generate heatmaps of  
513  $\delta^{15}\text{N}$  data distributions for specific time intervals. These heatmaps visualize the average spatial  
514 distribution of  $\delta^{15}\text{N}$  for any selected geological interval, offering preliminary validation for user  
515 hypotheses and aiding in uncovering the evolution of the global nitrogen cycle.

516 **7 Data availability**

517 The DSMS-NI version 0.3 can be accessed via Zenodo at <https://doi.org/10.5281/zenodo.15117375> (Du  
518 et al., 2025a) and via the GeoBiology website at <https://geobiologydata.cug.edu.cn/> (last access: April  
519 30 2025).

520 **8 Code availability**

521 The code used to validate the dataset, make the figures in this manuscript, and the heatmap tool is

522 available on Zenodo (<https://doi.org/10.5281/zenodo.15758073>). The paleocoordinates were estimated  
523 using the PointTracker v7 tool published by the PALEOMAP Project, which can be found at  
524 <http://www.paleogis.com> (last access: April 1 2025; <https://doi.org/10.13140/RG.2.1.2011.4162>,  
525 Scotese, 2008).

526 **Author contributions.** YD, HYS and HJS designed the study and secured funding. TJA, EES, SEG,  
527 JDC, YD, HZ, XKL, JP, YW, JK, XS, HS, DC and LT conducted data acquisition, curation and  
528 validation. YD, LW, JZ, QL, XCL and HY developed computational methodologies and provided  
529 technical support. YD prepared the paper with contribution from all co-authors.

530 **Competing interests.** The authors declare that they have no conflicts of interest.

531 **Acknowledgements.** This work has benefited from previous  $\delta^{15}\text{N}$  datasets compiled by Jan-Erik Tesdal,  
532 Christophe Thomazo, Thomas J. Algeo, Eva E. Stüeken, Magali Ader, Xinjiang Wang, and Michael A.  
533 Kipp.

534 **Financial support.** This work has been funded by the State Key R&D Project of China  
535 (2023YFF0804000), the National Natural Science Foundation of China (42172032; 42325202;  
536 42402316), the China Postdoctoral Science Foundation (2025T180107), the Postdoctoral Fellowship  
537 Program of CPSF (GZB20230679), the Postdoctoral Project of Hubei Province (2024HBBHCXB087),  
538 the Natural Science Foundation of Hubei Province (2023AFA006).

539 **References**

540 Ader, M., Thomazo, C., Sansjofre, P., Busigny, V., Papineau, D., Laffont, R., Cartigny, P., and  
541 Halverson, G. P.: Interpretation of the nitrogen isotopic composition of Precambrian sedimentary  
542 rocks: Assumptions and perspectives, *Chem. Geol.*, 429, 93–110,  
543 <https://doi.org/10.1016/j.chemgeo.2016.02.010>, 2016.

544 Algeo, T. J., Rowe, H., Hower, J. C., Schwark, L., Herrmann, A., Heckel, P.: Changes in ocean  
545 denitrification during Late Carboniferous glacial–interglacial cycles, *Nat. Geosci.*, 1(10), 709–714,  
546 <https://doi.org/10.1038/ngeo307>, 2008.

547 Algeo, T. J., Meyers, P. A., Robinson, R. S., Rowe, H., and Jiang, G. Q.: Icehouse–greenhouse

548 variations in marine denitrification, *Biogeosciences*, 11, 1273–1295,  
549 <https://doi.org/10.5194/bg-11-1273-2014>, 2014.

550 Altabet, M. A., Murray, D. W., and Prell, W. L.: Climatically linked oscillations in Arabian Sea  
551 denitrification over the past 1 m.y.: Implications for the marine N cycle, *Paleoceanography*, 14,  
552 732–743, <https://doi.org/10.1029/1999PA900035>, 1999.

553 Bebout, G. E., Cooper, D. C., Bradley, A. D., and Sadofsky, S. J.: Nitrogen-isotope record of fluid-rock  
554 interactions in the Skiddaw aureole and granite, English Lake District, *Am. Mineral.*, 84,  
555 1495–1505, <https://doi.org/10.2138/am-1999-1002>, 1999.

556 Bush, A. M. and Payne, J. L.: Biotic and Abiotic Controls on the Phanerozoic History of Marine  
557 Animal Biodiversity, *Annu. Rev. Ecol. Evol. Syst.*, 52, 269–289,  
558 <https://doi.org/10.1146/annurev-ecolsys-012021-035131>, 2021.

559 Busigny, V., Cartigny, P., Philippot, P., Ader, M., and Javoy, M.: Massive recycling of nitrogen and  
560 other fluid-mobile elements (K, Rb, Cs, H) in a cold slab environment: evidence from HP to UHP  
561 oceanic metasediments of the Schistes Lustrés nappe (western Alps, Europe), *Earth Planet. Sci.*  
562 *Lett.*, 215, 27–42, [https://doi.org/10.1016/S0012-821X\(03\)00453-9](https://doi.org/10.1016/S0012-821X(03)00453-9), 2003.

563 Chase, B. M., Niedermeyer, E. M., Boom, A., Carr, A. S., Chevalier, M., He, F., Meadows, M. E., Ogle,  
564 N., and Reimer, P. J.: Orbital controls on Namib Desert hydroclimate over the past 50,000 years,  
565 *Geology*, 47, 867–871, <https://doi.org/10.1130/G46334.1>, 2019.

566 Diepenbroek, M., Grobe, H., Reinke, M., Schindler, U., Schlitzer, R., Sieger, R., and Wefer, G.:  
567 PANGAEA—an information system for environmental sciences, *Comput. Geosci.*, 28, 1201–1210,  
568 [https://doi.org/10.1016/S0098-3004\(02\)00039-0](https://doi.org/10.1016/S0098-3004(02)00039-0), 2002.

569 Du, Y., Song, H.Y., Tong, J., Algeo, T. J., Li, Z., Song, H.J., and Huang, J.: Changes in productivity  
570 associated with algal-microbial shifts during the Early Triassic recovery of marine ecosystems,  
571 *Geol. Soc. Am. Bull.*, 133, 362–378, <https://doi.org/10.1130/B35510.1>, 2021.

572 Du, Y., Song, H.Y., Grasby, S. E., Xing, T., Song, H.J., Tian, L., Chu, D., Wu, Y., Dal Corso, J., Algeo,  
573 T. J., and Tong, J.: Recovery from persistent nutrient-N limitation following the Permian–Triassic  
574 mass extinction, *Earth Planet. Sci. Lett.*, 602, 117944, <https://doi.org/10.1016/j.epsl.2022.117944>,  
575 2023.

576 Du, Y., Song, H.Y., Stüeken, E. E., Grasby, S. E., Song, H.J., Tian, L., Chu, D., Dal Corso, J., Li, Z.,  
577 and Tong, J.: Large nitrogen cycle perturbations during the Early Triassic hyperthermal, *Geochim.  
578 Cosmochim. Acta*, 382, 13–25, <https://doi.org/10.1016/j.gca.2024.08.009>, 2024.

579 Du, Y., Song, H. Y., Algeo, T. J., Zhang, H., Peng, J., Wu, Y., Lai, J., Shu, X., Song, H. J., Wei, L.,  
580 Zhang, J., Stüeken, E. E., Grasby, S. E., Dal Corso, J., Dai, X., Chu, D., Tian, L., Liang, Q., Li, X.,  
581 Yao, H., and Song, H.: The global database of deep-time marine nitrogen isotope data [data set].  
582 Zenodo. <https://doi.org/10.5281/zenodo.15117375>, 2025a.

583 Du, Y., Song, H. Y., Algeo, T. J., Zhong, L., Li, J., and Song, H. J.: Tectonic controls on nitrogen  
584 cycling and ocean ventilation dynamics in the Late Cretaceous equatorial Atlantic, *Earth Planet.  
585 Sci. Lett.*, 667, 119517, <https://doi.org/10.1016/j.epsl.2025.119517>, 2025b.

586 Farrell, Ú. C., Samawi, R., Anjanappa, S., Klykov, R., Adeboye, O. O., Agic, H., Ahm, A.-S. C., Boag,  
587 T. H., Bowyer, F., Brocks, J. J., Brunoir, T. N., Canfield, D. E., Chen, X., Cheng, M., Clarkson, M.  
588 O., Cole, D. B., Cordie, D. R., Crockford, P. W., Cui, H., Dahl, T. W., Mouro, L. D., Dewing, K.,  
589 Dornbos, S. Q., Drabon, N., Dumoulin, J. A., Emmings, J. F., Endriga, C. R., Fraser, T. A., Gaines,  
590 R. R., Gaschnig, R. M., Gibson, T. M., Gilleaudeau, G. J., Gill, B. C., Goldberg, K., Guilbaud, R.,  
591 Halverson, G. P., Hammarlund, E. U., Hantsoo, K. G., Henderson, M. A., Hodgskiss, M. S. W.,  
592 Horner, T. J., Husson, J. M., Johnson, B., Kabanov, P., Brenhin Keller, C., Kimmig, J., Kipp, M.  
593 A., Knoll, A. H., Kreitsmann, T., Kunzmann, M., Kurzweil, F., LeRoy, M. A., Li, C., Lipp, A. G.,  
594 Loydell, D. K., Lu, X., Macdonald, F. A., Magnall, J. M., Mänd, K., Mehra, A., Melchin, M. J.,  
595 Miller, A. J., Mills, N. T., Mwinde, C. N., O'Connell, B., Och, L. M., Ossa Ossa, F., Pagès, A.,  
596 Paiste, K., Partin, C. A., Peters, S. E., Petrov, P., Playter, T. L., Plaza-Torres, S., Porter, S. M.,  
597 Poulton, S. W., Pruss, S. B., Richoz, S., Ritzer, S. R., Rooney, A. D., Sahoo, S. K., Schoepfer, S.  
598 D., Sclafani, J. A., Shen, Y., Shorttle, O., Slotznick, S. P., Smith, E. F., Spinks, S., Stockey, R. G.,  
599 Strauss, J. V., Stüeken, E. E., Tecklenburg, S., Thomson, D., Tosca, N. J., Uhlein, G. J., Vizcaíno,  
600 M. N., Wang, H., White, T., Wilby, P. R., et al.: The Sedimentary Geochemistry and  
601 Paleoenvironments Project, *Geobiology*, 19, 545–556, <https://doi.org/10.1111/gbi.12462>, 2021.

602 Gard, M., Hasterok, D., and Halpin, J. A.: Global whole-rock geochemical database compilation, *Earth  
603 Syst. Sci. Data*, 11, 1553–1566, <https://doi.org/10.5194/essd-11-1553-2019>, 2019.

604 Godfrey, L. V., Omta, A. W., Tziperman, E., Li, X., Hu, Y., and Falkowski, P. G.: Stability of the marine  
605 nitrogen cycle over the past 165 million years, *Nat. Commun.*, 16, 8982,  
606 <https://doi.org/10.1038/s41467-025-63604-x>, 2025.

607 Hammarlund, E. U., Smith, M. P., Rasmussen, J. A., Nielsen, A. T., Canfield, D. E., and Harper, D. A.  
608 T.: The Sirius Passet Lagerstätte of North Greenland-A geochemical window on early Cambrian  
609 low-oxygen environments and ecosystems, *Geobiology*, 17, 12–26,

610 <https://doi.org/10.1111/gbi.12315>, 2019.

611 Hendricks, G., Tkaczyk, D., Lin, J., and Feeney, P.: Crossref: The sustainable source of  
612 community-owned scholarly metadata, Quant. Sci. Stud., 1, 414–427,  
613 [https://doi.org/10.1162/qss\\_a\\_00022](https://doi.org/10.1162/qss_a_00022), 2020.

614 Hoefs, J.: Stable Isotope Geochemistry, Springer International Publishing, Berlin,  
615 <https://doi.org/10.1007/978-3-030-77692-3>, 2021.

616 Ishida, A., Hashizume, K., and Kakegawa, T.: Microbial nitrogen cycle enhanced by continental input  
617 recorded in the Gunflint Formation, Geochem. Persp. Let., 13–18,  
618 <https://doi.org/10.7185/geochemlet.1729>, 2017.

619 Jia, Y. and Kerrich, R.: Giant quartz vein systems in accretionary orogenic belts: the evidence for a  
620 metamorphic fluid origin from  $\delta^{15}\text{N}$  and  $\delta^{13}\text{C}$  studies, Earth Planet. Sci. Lett., 184, 211 – 224,  
621 [https://doi.org/10.1016/S0012-821X\(00\)00320-4](https://doi.org/10.1016/S0012-821X(00)00320-4), 2000.

622 Jenkyns, H. C.: Geochemistry of oceanic anoxic events, Geochem. Geophys. Geosyst., 11, Q03004,  
623 <https://doi.org/10.1029/2009GC002788>, 2010.

624 Judd, E. J., Bhattacharya, T., and Ivany, L. C.: A Dynamical Framework for Interpreting Ancient Sea  
625 Surface Temperatures, Geophys. Res. Lett., 47, e2020GL089044,  
626 <https://doi.org/10.1029/2020GL089044>, 2020.

627 Judd, E. J., Tierney, J. E., Lunt, D. J., Montañez, I. P., Huber, B. T., Wing, S. L., and Valdes, P. J.: A  
628 485-million-year history of Earth's surface temperature, Science, 385, eadk3705,  
629 <https://doi.org/10.1126/science.adk3705>, 2024.

630 Junium, C. K., Meyers, S. R., and Arthur, M. A.: Nitrogen cycle dynamics in the Late Cretaceous  
631 Greenhouse, Earth Planet. Sci. Lett., 481, 404–411, <https://doi.org/10.1016/j.epsl.2017.10.006>,  
632 2018.

633 Kipp, M. A., Stüeken, E. E., Yun, M., Bekker, A., and Buick, R.: Pervasive aerobic nitrogen cycling in  
634 the surface ocean across the Paleoproterozoic Era, Earth Planet. Sci. Lett., 500, 117–126,  
635 <https://doi.org/10.1016/j.epsl.2018.08.007>, 2018.

636 Knies, J., Grasby, S. E., Beauchamp, B., and Schubert, C. J.: Water mass denitrification during the  
637 latest Permian extinction in the Sverdrup Basin, Arctic Canada, Geology, 41, 167–170,  
638 <https://doi.org/10.1130/G33816.1>, 2013.

639 Kocsis, Á. T. and Scotese, C. R.: Mapping paleocoastlines and continental flooding during the  
640 Phanerozoic, Earth Sci. Rev., 213, 103463, <https://doi.org/10.1016/j.earscirev.2020.103463>, 2021.

641 Koehler, M. C., Stüeken, E. E., Hillier, S., and Prave, A. R.: Limitation of fixed nitrogen and deepening  
642 of the carbonate-compensation depth through the Hirnantian at Dob's Linn, Scotland, *Palaeogeogr.*  
643 *Palaeoclimatol. Palaeoecol.*, 534, 109321, <https://doi.org/10.1016/j.palaeo.2019.109321>, 2019.

644 Lai, J., Song, H. Y., Chu, D., Dal Corso, J., Sperling, E. A., Wu, Y., Liu, X., Wei, L., Li, M., Song, H. J.,  
645 Du, Y., Jia, E., Feng, Y., Song, H., Yu, W., Liang, Q., Li, X., and Yao, H.: Deep-time marine  
646 sedimentary element database, *Earth Syst. Sci. Data*, 17, 1613–1626,  
647 <https://doi.org/10.5194/essd-17-1613-2025>, 2025.

648 Li, J., Song, H. Y., Du, Y., Wignall, P. B., Bond, D. P. G., Grasby, S. E., Song, H. J., Dal Corso, J., Tian,  
649 L., and Chu, D.: Spatial and temporal heterogeneity of the marine nitrogen cycle during the  
650 end-Triassic mass extinction, *Chem. Geol.*, 682, 122752,  
651 <https://doi.org/10.1016/j.chemgeo.2025.122752>, 2025.

652 Li, W., Zhou, L., Lin, Y., Zhang, H., Zhang, Y., Wu, X., Stevens, C., Yang, Y., Wang, H., Fang, Y., and  
653 Liang, F.: Interdisciplinary study on dietary complexity in Central China during the Longshan  
654 Period (4.5–3.8 kaBP): New isotopic evidence from Wadian and Haojiatai, Henan Province, *The*  
655 *Holocene*, 31, 258–270, <https://doi.org/10.1177/0959683620970252>, 2021.

656 Liu, Y., Magnall, J. M., Gleeson, S. A., Bowyer, F., Poulton, S. W., and Zhang, J.: Spatio-temporal  
657 evolution of ocean redox and nitrogen cycling in the early Cambrian Yangtze ocean, *Chem. Geol.*,  
658 554, 119803, <https://doi.org/10.1016/j.chemgeo.2020.119803>, 2020.

659 Liu, Z., Altabet, M. A., and Herbert, T. D.: Plio-Pleistocene denitrification in the eastern tropical North  
660 Pacific: Intensification at 2.1 Ma, *Chem. Geol.*, 9, 2008GC002044,  
661 <https://doi.org/10.1029/2008GC002044>, 2008.

662 Macdonald, F. A., Swanson-Hysell, N. L., Park, Y., Lisiecki, L., and Jagoutz, O.: Arc-continent  
663 collisions in the tropics set earth's climate state, *Science*, 364, 181–184,  
664 <https://doi.org/10.1126/science.aav5300>, 2019.

665 Martin, A. N. and Stüeken, E. E.: Mechanisms of nitrogen isotope fractionation at an ancient black  
666 smoker in the 2.7 Ga Abitibi greenstone belt, Canada, *Geology*, 52,  
667 <https://doi.org/10.1130/G51689.1>, 2024.

668 Meyers, P. A., Yum, J.-G., and Wise, S. W.: Origins and maturity of organic matter in mid-Cretaceous  
669 black shales from ODP Site 1138 on the Kerguelen Plateau, *Mar. Pet. Geol.*, 26, 909–915,  
670 <https://doi.org/10.1016/j.marpetgeo.2008.09.003>, 2009.

671 Montañez, I., Norris, R., et al.: Understanding Earth's Deep Past: Lessons for Our Climate Future,

672 National Research Council, National Academy of Sciences, Washington, D.C., 2011.

673 Moretti, S., Auderset, A., Deutsch, C., Schmitz, R., Gerber, L., Thomas, E., Luciani, V., Petrizzo, M. R.,  
674 Schiebel, R., Tripati, A., Sexton, P., Norris, R., D'Onofrio, R., Zachos, J., Sigman, D. M., Haug, G.  
675 H., and Martínez-García, A.: Oxygen rise in the tropical upper ocean during the Paleocene-Eocene  
676 Thermal Maximum, *Science*, 383, 727–731, <https://doi.org/10.1126/science.adh4893>, 2024.

677 Murphy, E. M. A. and Salvador, A.: International Subcommission on Stratigraphic Classification of  
678 IUGS International Commission on Stratigraphy, *Episodes*, 22, 1999.

679 National Research Council: *Scientific Ocean Drilling: Accomplishments and Challenges*, National  
680 Academies Press, Washington, D.C., <https://doi.org/10.17226/13232>, 2011.

681 Nichols, G.: *Sedimentology and stratigraphy*, John Wiley & Sons, 2009.

682 Pellerin, A., Thomazo, C., Ader, M., Rossignol, C., Rego, E. S., Busigny, V., and Philippot, P.:  
683 Neoarchaean oxygen-based nitrogen cycle en route to the Great Oxidation Event, *Nature*,  
684 <https://doi.org/10.1038/s41586-024-07842-x>, 2024.

685 Percival, L. M. E., Marynowski, L., Baudin, F., Goderis, S., De Vleeschouwer, D., Rakociński, M.,  
686 Narkiewicz, K., Corradini, C., Da Silva, A. -C., and Claeys, P.: Combined Nitrogen-Isotope and  
687 Cyclostratigraphy Evidence for Temporal and Spatial Variability in Frasnian–Famennian  
688 Environmental Change, *Geochem. Geophys. Geosyst.*, 23, e2021GC010308,  
689 <https://doi.org/10.1029/2021GC010308>, 2022.

690 Peters, K. E.: Guidelines for Evaluating Petroleum Source Rock Using Programmed Pyrolysis, *AAPG*  
691 *Bull.*, 70, 318–329, 1986.

692 Poulton, S. W. and Canfield, D. E.: Development of a sequential extraction procedure for iron:  
693 implications for iron partitioning in continentally derived particulates, *Chem. Geol.*, 214, 209–221,  
694 <https://doi.org/10.1016/j.chemgeo.2004.09.003>, 2005.

695 Ren, H., Sigman, D. M., Thunell, R. C., and Prokopenko, M. G.: Nitrogen isotopic composition of  
696 planktonic foraminifera from the modern ocean and recent sediments, *Limnol. Oceanogr.*, 57,  
697 1011–1024, <https://doi.org/10.4319/lo.2012.57.4.1011>, 2012.

698 Ren, H., Sigman, D. M., Martínez-García, A., Anderson, R. F., Chen, M.-T., Ravelo, A. C., Straub, M.,  
699 Wong, G. T. F., and Haug, G. H.: Impact of glacial/interglacial sea level change on the ocean  
700 nitrogen cycle, *Proc. Natl. Acad. Sci. U.S.A.*, 114, <https://doi.org/10.1073/pnas.1701315114>, 2017.

701 Sahoo, S. K., Gilleaudeau, G. J., Wilson, K., Hart, B., Barnes, B. D., Faison, T., Bowman, A. R.,  
702 Larson, T. E., and Kaufman, A. J.: Basin-scale reconstruction of euxinia and Late Devonian mass

703 extinctions, *Nature*, 615, 640–645, <https://doi.org/10.1038/s41586-023-05716-2>, 2023.

704 705 706 707 708 709 710 711 712 713 714 715 716 717 718 719 720 721 722 723 724 725 726 727 728 729 730 731 732 733

Scotese, C.: The PALEOMAP Project PaleoAtlas for ArcGIS, version 1, 2, 16–31, ResearchGate [data set]. <https://doi.org/10.13140/RG.2.1.2011.4162>, 2008.

Scotese, C. R. and Wright, N.: PALEOMAP Paleodigital Elevation Models (PaleoDEMs) for the Phanerozoic PALEOMAP Project, <https://www.earthbyte.org/paleodem-resource-scotese-and-wright-2018/> (last access: 1 April 2025), 2018.

Smart, S. M., Ren, H., Fawcett, S. E., Schiebel, R., Conte, M., Rafter, P. A., Ellis, K. K., Weigand, M. A., Oleynik, S., Haug, G. H., and Sigman, D. M.: Ground-truthing the planktic foraminifer-bound nitrogen isotope paleo-proxy in the Sargasso Sea, *Geochim. Cosmochim. Acta*, 235, 463–482, <https://doi.org/10.1016/j.gca.2018.05.023>, 2018.

Song, H.Y., Xing, T., Stüeken, E. E., Du, Y., Zhu, Y., Tao, X., Ni, Q., and Song, H.J.: Isotopic differences and paleoenvironmental significance of nitrogen contained in bulk sedimentary rocks, decarbonated aliquots and kerogen extracts, *Chem. Geol.*, 631, 121522, <https://doi.org/10.1016/j.chemgeo.2023.121522>, 2023.

Stüeken, E. E., Kipp, M. A., Koehler, M. C., and Buick, R.: The evolution of Earth's biogeochemical nitrogen cycle, *Earth Sci. Rev.*, 160, 220–239, <https://doi.org/10.1016/j.earscirev.2016.07.007>, 2016.

Stüeken, E. E., Pellerin, A., Thomazo, C., Johnson, B. W., Duncanson, S., and Schoepfer, S. D.: Marine biogeochemical nitrogen cycling through Earth's history, *Nat. Rev. Earth Environ.*, <https://doi.org/10.1038/s43017-024-00591-5>, 2024.

Sun, Y.: Dynamics of nutrient cycles in the Permian–Triassic oceans, *Earth Sci. Rev.*, 258, 104914, <https://doi.org/10.1016/j.earscirev.2024.104914>, 2024.

Tesdal, J.-E., Galbraith, E. D., and Kienast, M.: Nitrogen isotopes in bulk marine sediment: linking seafloor observations with subseafloor records, *Biogeosciences*, 10, 101–118, <https://doi.org/10.5194/bg-10-101-2013>, 2013.

Thomazo, C., Ader, M., and Philippot, P.: Extreme  $^{15}\text{N}$ -enrichments in 2.72-Gyr-old sediments: evidence for a turning point in the nitrogen cycle, *Geobiology*, 9, 107–120, <https://doi.org/10.1111/j.1472-4669.2011.00271.x>, 2011.

Tribouillard, N., Algeo, T. J., Lyons, T., and Riboulleau, A.: Trace metals as paleoredox and paleoproductivity proxies: An update, *Chem. Geol.*, 232, 12–32,

734 <https://doi.org/10.1016/j.chemgeo.2006.02.012>, 2006.

735 Tucker, M. E. and Wright, V. P.: *Carbonate Sedimentology*, John Wiley & Sons, 2009.

736 Uveges, B. T., Izon, G., Junium, C. K., Ono, S., and Summons, R. E.: Aerobic nitrogen cycle 100 My  
737 before permanent atmospheric oxygenation, *Proc. Natl. Acad. Sci.*, 122, e2423481122,  
738 <https://doi.org/10.1073/pnas.2423481122>, 2025.

739 Wang, D., Ling, H.-F., Struck, U., Zhu, X.-K., Zhu, M., He, T., Yang, B., Gamper, A., and Shields, G.  
740 A.: Coupling of ocean redox and animal evolution during the Ediacaran-Cambrian transition, *Nat.*  
741 *Commun.*, 9, 2575, <https://doi.org/10.1038/s41467-018-04980-5>, 2018.

742 Wang, X., Shi, X., Tang, D., and Zhang, W.: Nitrogen isotope evidence for redox variations at the  
743 Ediacaran-Cambrian Transition in South China, *J. Geol.*, 121, 489–502,  
744 <https://doi.org/10.1086/671396>, 2013.

745 Wang, X. T., Wang, Y., Auderset, A., Sigman, D. M., Ren, H., Martínez-García, A., Haug, G. H., Su, Z.,  
746 Zhang, Y. G., Rasmussen, B., Sessions, A. L., and Fischer, W. W.: Oceanic nutrient rise and the  
747 late Miocene inception of Pacific oxygen-deficient zones, *Proc. Natl. Acad. Sci. U.S.A.*, 119,  
748 e2204986119, <https://doi.org/10.1073/pnas.2204986119>, 2022.

749 Wilkinson, M. D., Dumontier, M., Sansone, S.-A., Bonino Da Silva Santos, L. O., Prieto, M., Batista,  
750 D., McQuilton, P., Kuhn, T., Rocca-Serra, P., Crosas, M., and Schultes, E.: Evaluating FAIR  
751 maturity through a scalable, automated, community-governed framework, *Sci. Data*, 6, 174,  
752 <https://doi.org/10.1038/s41597-019-0184-5>, 2019.

753 Winter, J. D.: *Principles of igneous and metamorphic petrology*, Pearson education Harlow, UK, 2014.

754 Xia, L., Cao, J., Stüeken, E. E., Hu, W., and Zhi, D.: Linkages between nitrogen cycling, nitrogen  
755 isotopes, and environmental properties in paleo-lake basins, *GSA Bull.*, 134, 2359–2372,  
756 <https://doi.org/10.1130/B36290.1>, 2022.

757 Zhong, L., Peng, J., He, J., Du, Y., Xing, T., Li, J., Guo, W., Ni, Q., Hu, J., and Song, H.Y.:  
758 Optimizations of the EA-IRMS system for  $\delta^{15}\text{N}$  analysis of trace nitrogen, *Appl. Geochem.*, 159,  
759 105832, <https://doi.org/10.1016/j.apgeochem.2023.105832>, 2023.